Journal of Engineering Physics and Thermophysics, Vol. 81, No. 2, 2008

QUANTITATIVE VISUALIZATION OF ULTRASONIC ACOUSTIC WAVES BY MEANS OF DIGITAL LASER SPECKLE-TECHNOLOGIES

C. A. Greated,[a] J. A. Cosgrove,[b] and N. A. Fomin[c]

UDC 535.241.13:534

An original version of digital laser speckle photography has been used for visualization and quantitative diagnosis of acoustic waves in liquids in the megahertz frequency range. Standing acoustic waves were generated in tanks of special configuration which permitted obtaining analytical dependences of refraction angles of the probe laser radiation on the wave intensity. These refraction angles were determined experimentally by the change in contrast of the speckle fields arising in the scattered probe radiation and recorded by means of high-resolution digital CCD matrices. Quantitative diagnosis of the pressure and velocity fields in acoustic waves was carried out by measuring the deformation of the laser intensity correlation functions in recorded speckle fields.

Introduction. Visualization of shock and acoustic waves has a long history starting from the experiments of Toepler, Mach, and Salcher [1, 2]. In these experiments, August Toepler managed for the first time to visualize and sketch a shock wave generated by electric discharge in a liquid [1], and Ernest Mach and Peter Salcher photographed a shock wave in the air near a bullet flying at supersonic speed [2]. The qualitative transition from sketches of visualizing images to their "objective" photochronography became possible due to advances in the photographic recording of images in the experiments of Fox Talbot, one of the inventors of photography [3]. A more comprehensive historical survey of the application of optical methods of visualization of flows and their analysis, beginning with the experiments of Robert Hooke and J.-P. Marat in the 17th century up to now, is contained in monograph [4]. The fundamental and generalizing works and monographs [5–9] are devoted to the description of the application of visualization techniques for investigating acoustic and shock waves. Traditionally, visualization of shock-wave flows has a qualitative character, and attempts to make a quantitative diagnosis of such flows with the use of two-dimensional or three-dimensional visualization are very sparse.

As with the investigations of many other processes, a powerful impetus to the development of optical methods for diagnosing fast processes has been the discovery and wide adoption in measurement practice of laser systems and digital recorders with high spatial resolution based on CCD matrices and structures [10, 11]. One of the first diagnostic techniques for flows using the coherent properties of the laser radiation was laser Doppler anemometry (LDA) [12, 13]. As a new technique for laser anemometry of flows (PIV*), LDA is based on the introduction into the flow being investigated for visualizing particles which should completely "trace" the flow being investigated. While LDA registers the Doppler shift of the frequency of the probing laser radiation scattered by moving particles, the PIV technique is based on the statistical analysis of the shifts of images of particles visualizing the flow being investigated in a finite time interval in recording these particles in a selected plane by means of a photographic plate or a CCD camera [14, 15]. Unlike LDA, PIV permits simultaneous measurements throughout the flow field within the limits of the selected laser plane ("laser knife"). Despite the great advances of this technique in investigating many flows, including hypersonic ones, its application for diagnosing ultrasonic high-frequency waves is limited by the capabilities of laser systems, as well as by the sizes (inertia) of visualizing particles introduced into the flow being investigated [16–19].

*PIV (particle image velocimetry) — anemometry using analysis of images of visualizing particles.

[a]University of Edinburgh, Edinburgh, Scotland, UK; [b]Professional Scientific Limited, Edinburgh Technology Transfer Centre BioSpace, Edinburgh, Scotland, UK; [c]A. V. Luikov Heat and Mass Transfer Institute, National Academy of Sciences of Belarus, 15 P. Brovka Str., Minsk, 220072; email: fomin@hmti.ac.by. Translated from Inzhenerno-Fizicheskii Zhurnal, Vol. 81, No. 2, pp. 229–239, March–April, 2008. Original article submitted November 25, 2007.

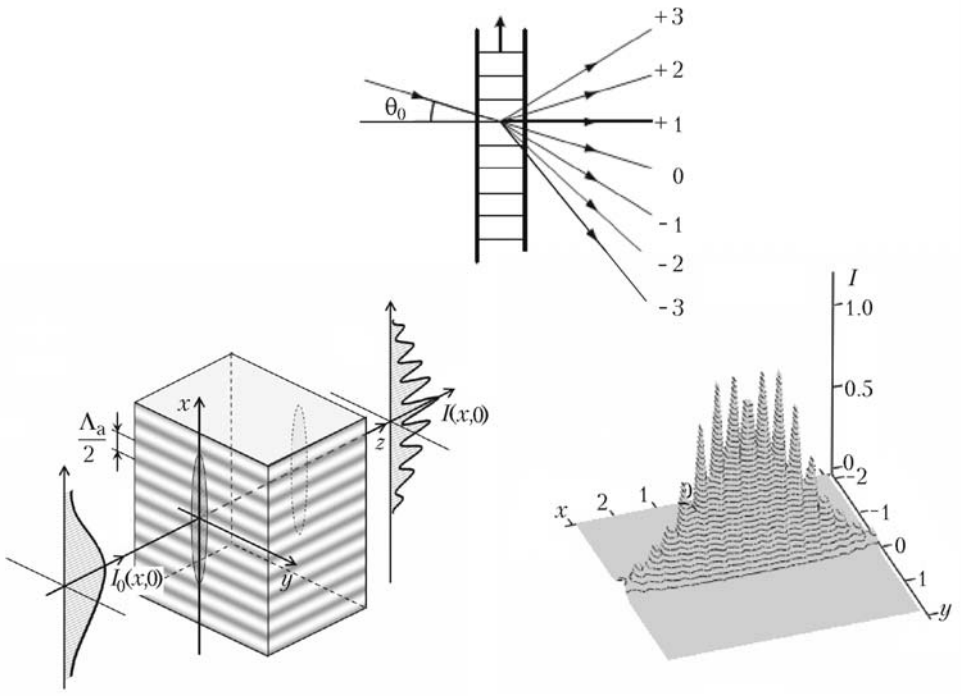

Fig. 1. Illustration of the Raman–Nath diffraction and calculation of the diffraction pattern for the elliptic form of the probing laser radiation according to the data of [38]. x, y, mm; I, rel. units.

The alternative flow visualization techniques are based on the recording of phase inhomogeneities of the flow. Such methods do not require the introduction of visualizing particles and are based on the line-in-sight probing of investigated flows. Among them are shadow methods, holography, and interferometry, including speckle and Talbot interferometry. The latter have proved to be the most suitable for the change-over to digital recording systems. They are also promising for use in investigations of ultrasonic waves [20].

The present paper generalizes the experience of using the new technologies of digital laser speckle interferometry (DLSI) for quantitative diagnosis of ultrasonic flows [21–23]. The proposed DLSI method is based on the recording of the probing radiation refraction by optical inhomogeneities in acoustic fields and does not require the introduction into the flow being investigated of visualizing particles. Digital recording of speckle fields of the laser radiation upon its interaction with an acoustic wave permits precision analysis of the microstructure of such fields and quantitative determination of the deformations of speckle fields caused by the refraction, from which the local amplitude of the acoustic wave is determined simultaneously throughout the flow field. Three-dimensional acoustic waves are reconstructed by means of Radon transforms and integrated optical data obtained simultaneously for various probing angles [24, 25].

Laser Probing of Acoustic Fields. Let a standing acoustic wave be located in a region $z \geq 0$ (Fig. 1). Collimated laser radiation with a wavelength λ is probing this medium. The acoustic wave causes fluctuations of the refractive index. For acoustic waves in fluids these fluctuations are caused by pressure fluctuations: $\Delta n(y, t) = \beta \Delta p(y, t)$, where $\beta = \dfrac{\partial n}{\partial p}$ is the piezooptical coefficient. For water at $\lambda = 633$ nm $\beta = 1.2 \cdot 10^{-14} T^2 - 1 \cdot 10^{-12} T + 1.638 \cdot 10^{-10}$ (in Pa^{-1}) (see [26, 27]). At $T = 17.0^{\circ}\text{C}$ $\beta = 1.503 \cdot 10^{-10}$ Pa^{-1}.

The instantaneous pressure distribution in the standing acoustic wave in the one-dimensional approximation is described by the relation

$$\Delta p\,(y, t) = 2\Delta p_0 \sin(ky + \varphi_0) \cos \omega t\,, \tag{1}$$

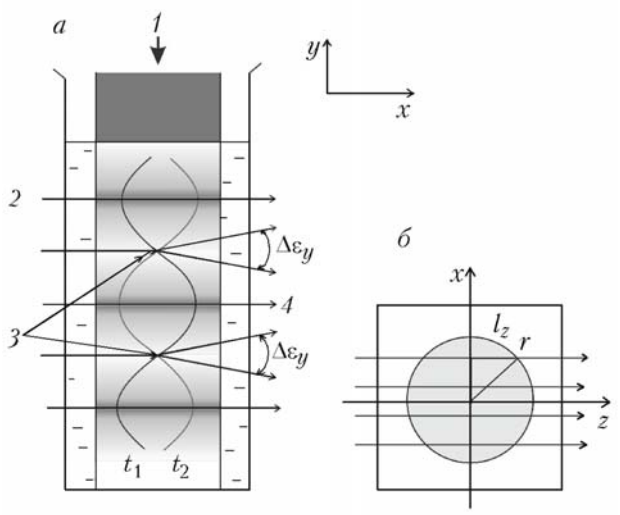

Fig. 2. Pressure distribution at times t_1 and t_2 in a standing acoustic wave in the fluid in a circular glass pipe placed in a rectangular tank filled with a fluid with a refractive index equal to the refractive index of the glass: 1) acoustic generator; 2) collimated probing radiation; 3) acoustic wave nodes; 4) direction of the probing radiation to the speckle field generator.

where k is the acoustic wave vector magnitude, $|\mathbf{k}| = \frac{2\pi}{\Lambda_a}$; Δp_0 is the amplitude of pressure changes in the acoustic wave. Accordingly, the spatial and temporal changes in the refractive index will have the following form:

$$\Delta n\,(y) = 2\beta\Delta p_0\,(\sin\,(ky + \varphi_0))\,, \quad \Delta n\,(t) = 2\beta\Delta p_0 \cos\omega t\,.$$

It is these changes that cause diffraction and refraction of the radiation transmitted through the investigated medium. For an optically thin layer, the influence of the refraction processes is weak, and the diffraction pattern of the interaction between the laser radiation and an acoustic wave can be constructed in the Raman–Nath approximation where perturbations of the refractive index in the acoustic are considered as a diffraction grating with a spacing equal to the acoustic wavelength [28, 29]. The deflection angle for the diffraction order m is of the form

$$\theta_m = \sin\theta_0 + \frac{m\lambda}{\Lambda_a n_0}\,, \quad m = 0,\ \pm 1,\ \ldots\,,$$

where θ_0 is the angle of incidence of the probing radiation; Λ_a is the wavelength of acoustic oscillations; n_0 is the refractive index of the medium. The intensity distribution in the diffraction region is described by Bessel functions $I_{\pm m} = J_m^2(\zeta)$, where ζ is the Raman–Nath parameter, $\zeta = 4\pi\Delta n_0 l_z/\lambda$; $\Delta n_0 = \beta\Delta p_0$ is the amplitude of changes in the refractive index in the acoustic wave; $2l_z$ is the optical path; J_m stands for Bessel functions of order m. The Raman–Nath approximation holds for small optical perturbations when the value of $\zeta << 1$. For larger optical thicknesses, the determination of the coordinate dependences of intensity in both the far and near diffraction regions becomes much more difficult [30–34]. At the same time, using a theoretical description of the diffraction pattern of the interaction between the probing laser radiation and the acoustic wave, Reibold et al. managed to reconstruct the three-dimensional pattern of an ultrasonic wave from data on multiaspect measurements of its intensity in the diffraction region up to numbers $\zeta \simeq 2.4$ [35–37]. B. S. Rinkevichius et al. succeeded in constructing the laser radiation intensity distribution in the diffraction region for a laser radiation of elliptic form characteristic of the "laser knife" diagnostics [38].

For the geometry presented in Fig. 2, it is possible to obtain the integral of the optical perturbation along the probing laser beam in analytical form and relate the refraction angle of laser radiation to the local amplitude of the pressure change in the sound wave. For a spatially homogeneous acoustic wave in the plane (x, z) taking into account that the optical path is equal to $2l_z = 2\sqrt{r^2 - x^2}$ and that

$$\frac{\partial n}{\partial y}(y, t) = 2\beta\Delta p_0 k \cos(ky + \varphi_0) \cos \omega t ,$$

the integral along the optical path is calculated analytically:

$$\varepsilon_y = \int_{-l_z}^{l_z} \frac{1}{n_0} \frac{\partial n}{\partial y} dz = 2l_z \frac{\partial n}{n_0 \partial y} .$$

The dependence of the deflection angle of the probing radiation in the plane (x, y) is described by the expression

$$\varepsilon_y(x, y) = 2\sqrt{r^2 - x^2}\, k \frac{\partial n}{n_0 \partial y} = \frac{4\beta\Delta p_0 k}{n_0} \sqrt{r^2 - x^2} \cos(ky + \varphi_0) .$$

Thus, maximal deflection angles of the probing radiation are attained in acoustic wave nodes, whereas in the region with the maximum value of the amplitude the probing radiation is transmitted without deflections (see Fig. 2a). The deflection angle at each point is directly proportional to the wave amplitude at a point with a phase $\varphi = \varphi_0 + \pi/2$. At a comparatively long-term registration of probing radiation deflection angles during many acoustic cycles the speckle field contrast at the points corresponding to the acoustic wave nodes will soften because of the elongation of speckles in the direction of refraction leading to a deformation ("smearing") of the speckles. For acoustic pressure $\Delta p = 10^5$ Pa, the probing radiation deflection angles are of the order of 10^{-5} rad and can be well determined by the DLSI methods. The trajectories of laser beams in acoustic waves can be described more exactly within the framework of the approximation of geometrical optics on the basis of solving the eikonal equation

$$\frac{d}{ds}\left[n_{\text{a}}(\mathbf{r}) \frac{d\mathbf{r}}{ds} \right] = \nabla n_{\text{a}}(\mathbf{r}) ,$$

where $n_{\text{a}} = \dfrac{c}{c_\infty}$ is the acoustic refractive index. Such a numerical tracing of the laser radiation in three-dimensional acoustic waves is described in [39].

Experimental Technique. One of the basic optical configurations of DLSI is illustrated in Fig. 3. Collimated laser radiation is directed onto the medium being investigated, as a result of the interaction with which a medium-distorted wavefront characterized at each point by the refraction angle $\varepsilon(x, y)$ is formed at the output. This wavefront is projected on a matte plate behind which a speckle field is formed as a result of the interference in the diffusion radiation. This field in some plane separated from the matte plate by distance L is projected on the image plane in which a sensitive matrix of the CCD camera is placed. The positions of individual speckles in the plane 8 (Fig. 3) shift for distance $\Delta = \varepsilon(x, y)L$ because of the wavefront distortion in the investigated medium, and in the recording region the value of this shift will be equal to $M\Delta = M\varepsilon(x, y)L$, where M is the optical magnification of the image by the lens 9 in Fig. 3. The value of this shift in each pixel of the CCD camera matrix can be measured with very high accuracy by means of auto- and cross-correlation analysis, as will be shown below. This analysis is carried out as in the widely known PIV technique where shifts of particle images in the time between exposures are determined. As mentioned above, the fundamental difference of DLSI from PIV is that DLSI does not require the introduction of visualizing particles into the investigated flow. This difference becomes particularly important in investigating ultrafast flows when the inertia of particles, however small, becomes appreciable. An analog of particles in the DLSI technique are virtual particles — light speckles having no inertia. An important feature of DLSI is also the easy variation of speckle sizes in a facility by means of optical alignment. The size of speckles therewith can easily be changed by several orders of magnitude beginning with the minimum size determined by the probing laser radiation wavelength, which is usually about 1 μm.

In recording speckle fields, two different modes are possible:

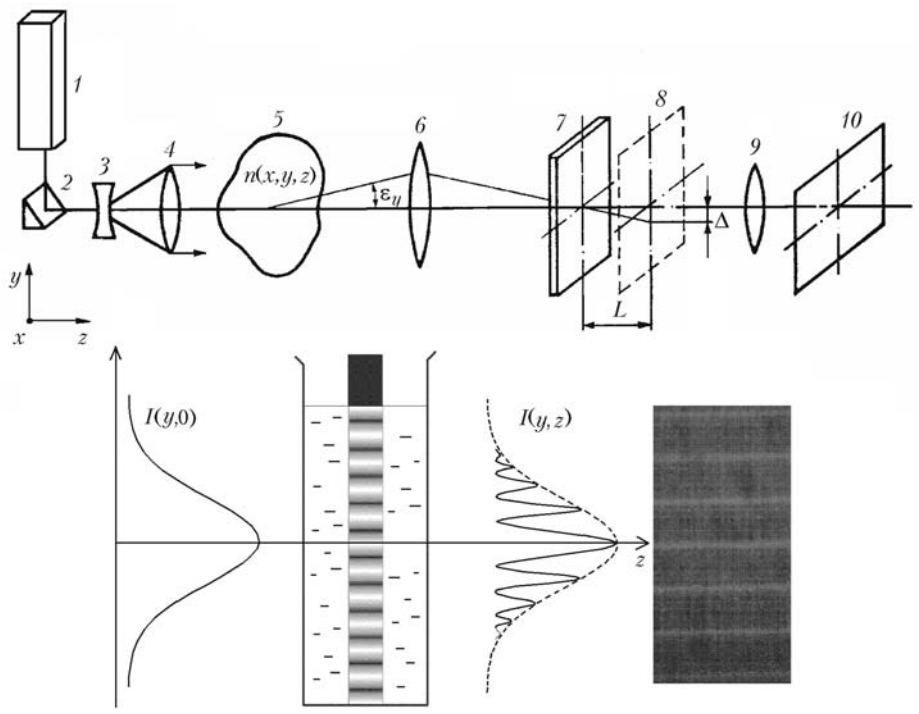

Fig. 3. Optical scheme of DLSI and example of the diffraction pattern in acoustic wave probing by collimated laser radiation: 1) probing laser; 2) deflecting prism; 3, 4) collimators; 5) investigated object; 6) matching lens; 7) matte plate; 8) speckle field image plane; 9) imaging lens; 10) recording plane.

1) continuous recording when the speckle field is recorded for a long time compared to the characteristic time of the process being investigated (such a mode is referred to as the single-exposure mode — the deformation of speckles caused by their shifts during the exposure is recorded);

2) two- or multiexposure recording in which the position of speckles are recorded in the process of short ("instantaneous") exposures at different instants of time (this regime is more accurate but its realization requires special double- or multipulse lasers with short lasing pulses and the possibility of varying the interpulse delay).

In the present work, we used single-exposure recording with sound wave probing by a cw He–Ne laser. The speckle-field deformation was recorded in the exposure period determined by the mechanical shutter of the CCD camera. For an exposure time of 1 msec at a sound wave frequency of 1 MHz we measured the averaged deformation of speckles in 1000 acoustic cycles.

Digital Speckle Image Processing. The algorithm of single-exposure speckle-image processing developed by us consists of determining the averaged deformation of speckles in each small singled-out window (zone) of the CCD matrix by calculating the two-dimensional autocorrelation function of this image, also referred to as the specklogram. To this end, the image obtained is broken down into small subregions (averaging windows), in each of which the autocorrelation function is calculated depending on the digital coordinates (pixels of the CCD matrix) in this subregion (m, n). With allowance for the experimental noise in each such zone of the specklogram $\tilde{\sigma}(m, n)$ the autocorrelation function represents the convolution of the corresponding laser radiation intensities in the speckle field:

$$\mathfrak{I}(m, n) = I(m, n) \otimes I^{*}(m, n) + \tilde{\sigma}(m, n). \tag{2}$$

In the Fourier plane, this relation has the form

$$\mathbb{F}\{\mathfrak{I}\}(u, v) = \mathbb{F}\{I\}(u, v) \bullet \mathbb{F}\{I^{*}\}(u, v) + \sigma(u, v), \tag{3}$$

and the estimate of the sought autocorrelation function $\tilde{\mathfrak{I}}$ can be obtained by the relation

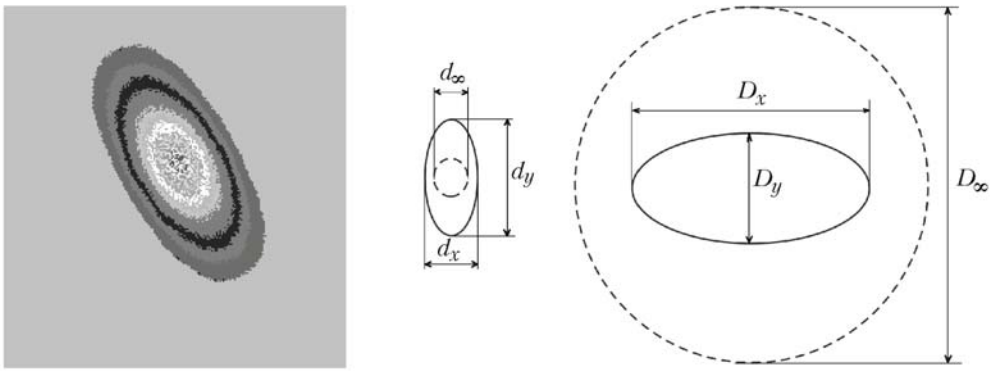

Fig. 4. PC-synthesized diffraction halo of the single-exposure specklogram and basic notation used in its analysis; d_∞, averaged diameter of the speckle in the unperturbed region; $d_{x,y}$, averaged speckle sizes on the x- and y-coordinates, respectively, at the investigated point (zone), D_∞, diffraction halo diameter in the unperturbed region, $D_{x,y}$, diffraction halo sizes on the x- and y-coordinates, respectively, at the investigated point.

$$\mathfrak{I}(m, n) = \mathbb{F}^{-1}\left\{\mathbb{F}\{\tilde{I}\}(u, v) \bullet \mathbb{F}\{\tilde{I}^*\}(u, v)\right\}. \tag{4}$$

Function (2) and its estimate $\tilde{\mathfrak{I}}(m, n)$ can also be calculated by direct comparison of the corresponding intensities on the CCD matrix:

$$\mathfrak{I}(m, n) = \frac{MN}{(M-m)(N-n)}\left[\frac{\sum_{p=1}^{M-mN-n}\sum_{q=1} I(p, q)\, I(m+p, n+q)}{\sum_{p=1}^{M}\sum_{q=1}^{N} I(p, q)\, I(p, q)}\right].$$

The Fourier transform of a single-exposure specklogram can be taken optically. In this case, it represents a diffraction halo formed behind the specklogram upon its scanning by a laser beam. Unlike the double-exposure specklogram, the halo is not modulated by the interference fringes and represents a circle for the ideal speckle field recorded with the use of a short exposure, or an ellipse for the deformed speckle field with the semimajor axis orthogonal to the direction of the predominant shift of speckles in the process of exposure, whose duration is comparable to the characteristic time of the process being investigated (Fig. 4). Because of the statistical character of calculations by relations (2)–(4) and natural filtration in averaging over large experimental data arrays, the sought value of the speckle deformation $|\Delta^2| = (d_x - d_\infty)^2 + (d_y - d_\infty)^2$ is determined with a very high (subpixel) accuracy even for high-noise specklograms, which permits quantitative determination of the sought two-dimensional field with a high spatial resolution determined by a large number of flow points at which the velocity vector has been calculated. So, in using a high-resolution CCD camera (e.g., 4000 × 4000 pixels) and averaging over subregions with size of 10 × 10 pixels, the number of such points can amount to 160,000. Precisely this important feature of the DLSI method makes it possible to perform a statistical analysis of the measurement data and determine the dynamic correlation characteristics of complex flows, which are unavailable when obtaining information at a limited number of flow points.

The parameters directly measured in each window of the specklogram are the ellipse semiaxes of the diffraction halo (a, b) or their projections on the coordinate axes D_x, D_y. As mentioned above, these quantities or, to be more exact, their differences from the diameter of the diffraction halo of the initial speckle field D_∞ are proportional to the window-averaged increase in the sizes (elongation) of speckles along the corresponding orthogonal axes. We have shown [40] that the sought deformation of speckles is equal to

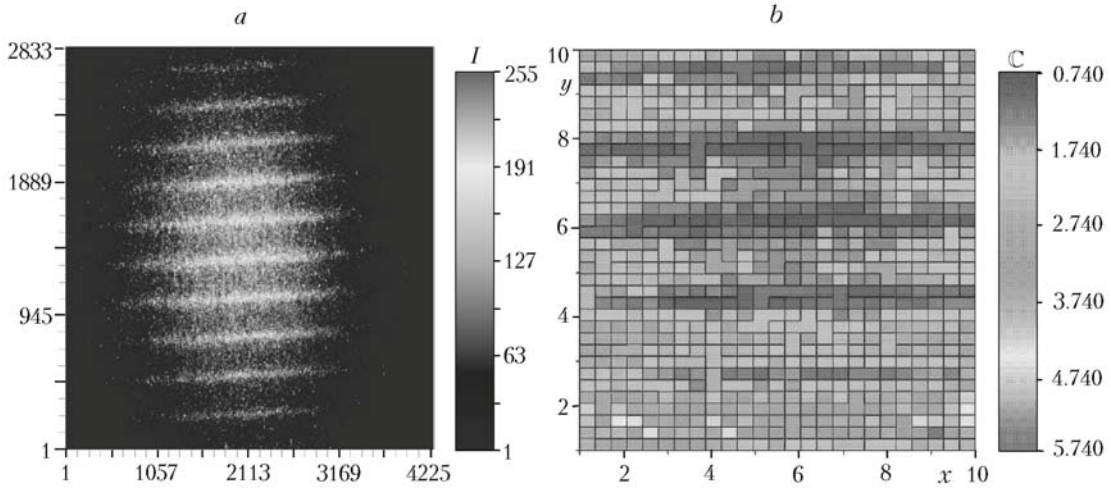

Fig. 5. Laser radiation intensity distribution (in arbitrary units) in the region of the diffraction halo (a) and calculated contrast of the speckle field in standing acoustic wave probing in water (b).

$$\Delta d_x = C\frac{D_\infty - D_x}{D_x}, \quad \Delta d_y = C\frac{D_\infty - D_y}{D_y},$$

where C is a normalization constant, which can be taken as a unit.

Another measured parameter of the single-exposure specklogram is the speckle field contrast. The contrast value is different in different subregions of the specklogram and appears to be inversely proportional to the deformation of speckles at a corresponding point during the exposure. This value can also be determined by direct calculation by the formula $\mathbb{C}(m, n) = \dfrac{\sigma_1(m, n)}{\langle I(m, n)\rangle}$, where $\sigma_1(m, n)$ is the rms deviation of the intensity in a given subregion of the speckle field. In the ideal speckle field, this value is equal to the mean intensity of the field $\sigma_1(m, n) = \langle I(m, n)\rangle$, with the contrast $\mathbb{C}(m, n) = 1$. When the statistics is disturbed, e.g., because of the shift of speckles during the exposure, the field contrast changes and one can also determine by the value of this contrast the sought deformation of speckles. Such a principle of measurements is widely used in combinations of the PIV technique and speckle photography in diagnosing microshifts in mechanics [41] and botany [42], as well as in investigating the microcirculation of blood in patients *in vivo* [43–46].

Results and Discussion. Figure 5 shows an example of the diffraction halo in probing a standing acoustic wave with a frequency of 1 MHz in water obtained with the aid of a cw He–Ne laser. The photograph of the halo was taken with an exposure containing 1000 acoustic cycles. Such a pattern is visually observed for a long time, which points to a good stabilization of the wave. As mentioned above, the obtained laser intensity distribution in combination with a detailed theoretical analysis of the diffraction process can be used directly for quantitative diagnostics of the wave. The quantitative data on the acoustic waves obtained below do not require such a detailed theoretical description of the diffraction process and are based on the statistical analysis of the microstructure of the diffraction halo described in the previous section. For instance, Fig. 5b shows the calculated speckle field contrast distribution modulating the diffraction pattern obtained. Quantitative measurements of the acoustic wave amplitude by the speckle field contrast require experimental calibration. Such calibration is analogous to the calibration of speckle velocimeters and was carried out earlier in real-time visualization of the near-surface blood flow in human tissues *in vivo* [44]. It was shown that the accuracy of determining the deformation of speckles by analyzing the speckle field contrast is of the order of 10–15%. The deformation of speckles can be measured with a much higher accuracy by analyzing the form of the autocorrelation function of the speckle field. Generally speaking, this method does not require calibration, since the sought deformation can be measured absolutely in pixel sizes of the CCD matrix. However, for convenience and verification of quantitative measurements, we carried out calibration with the use of a rotating matte plate as a gener-

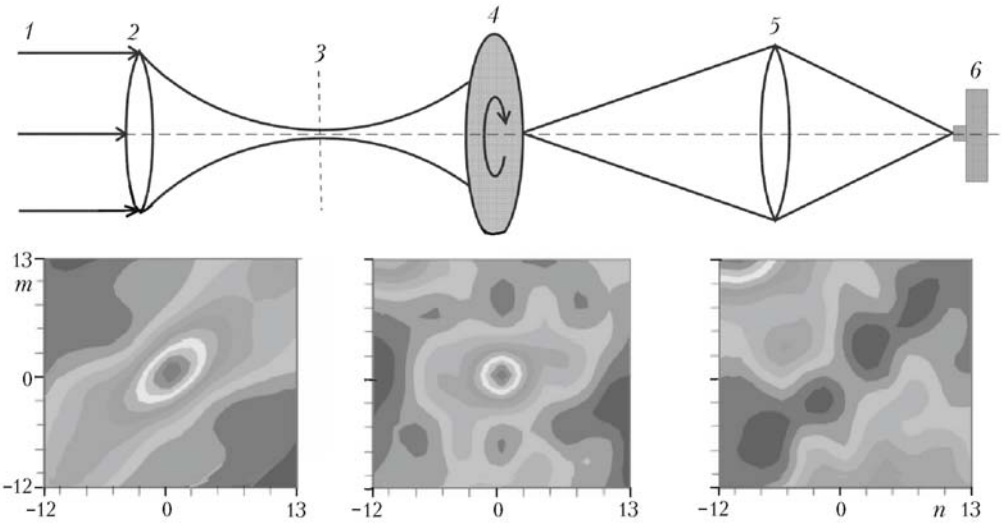

Fig. 6. Optical configuration for dynamic calibration of DLSI and samples of obtained autocorrelation functions: 1) collimated laser radiation; 2) lens forming a laser beam waist 3; 4) rotating matte plate; 5) lens of the CCD camera; 6) high-resolution CCD matrix.

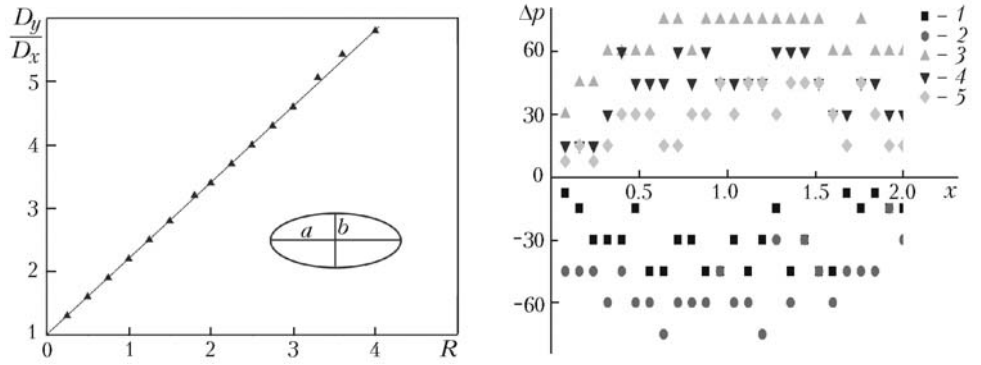

Fig. 7. Calibration results of the single-exposure scheme of DLSI (R, coordinate along the radius of the rotating disk) and measured pressure distributions in a standing acoustic wave with a frequency of 3 MHz for different wave phases: 1) $\varphi = 3\pi/4$; 2) π; 3) 0; 4) $\pi/8$; 5) $3\pi/8$. Δp, kPa; x, R, cm.

ator of "calibrated" elongations of speckles (Figs. 6–8). Check of the operating capacity of the single-exposure scheme and its dynamic calibration were performed when recording moving speckle fields generated by a rotating disk made of matte glass. The exposure time was chosen so that the relative elongation of speckles was varied from 0.1 in the central region of the disk to 5–10 at its periphery.

Figure 6 shows the evolution of the autocorrelation functions of the rotating disk specklogram (lower part of the figure) as the averaging window moved from the center of the disk to its periphery. The velocity profile obtained for the rotating disk with a good accuracy is linear, which conforms to the chosen model of motion. Velocity measurements are taken simultaneously at 88 points ("subregions"), which permits obtaining two-dimensional information simultaneously throughout the flow field.

The calibration results presented in Fig. 7 show that the velocity dependence of the relative elongation of speckles is practically linear in the range $\Delta d/d_\infty = 0.25$–5, which corresponds to the dynamic measurement range of ~20. This value is very close to the corresponding dynamic measurement range of the method of the double-exposure PIV technique and speckle photography. For the double-exposure PIV technique this range can easily be adapted to the investigated flow by varying the time between exposures, and for the single-exposure technique by selecting speckle sizes at a "short" exposure (d_∞).

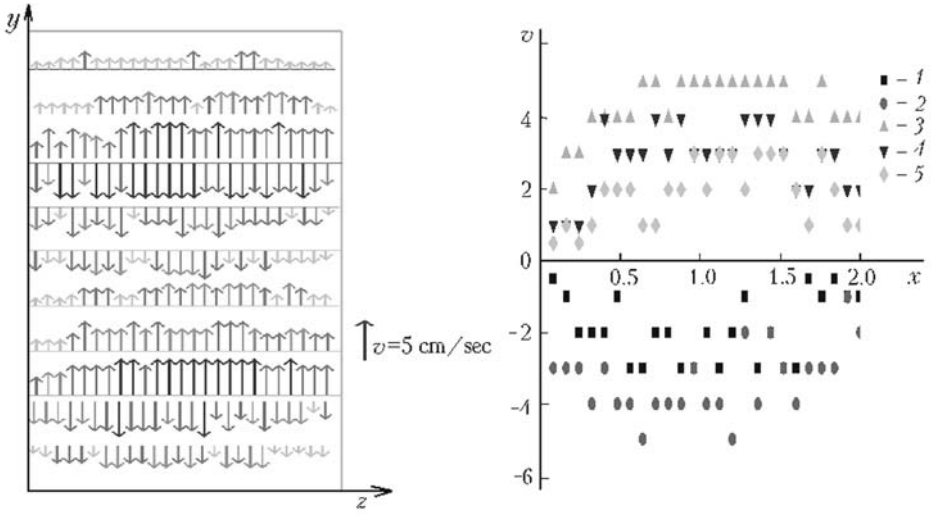

Fig. 8. Velocity fields calculated by the measured pressure distributions in an acoustic wave with a frequency of 3 MHz for different wave phases [1) $\varphi = 3\pi/4$; 2) π; 3) 0; 4) $\pi/8$; 5) $3\pi/8$] and velocity distributions for different cross-sections of the acoustic wave. v, cm/sec; x, cm.

Conclusions. Analysis of the data obtained shows that the single-exposure scheme of DLSI provides reliable measurements of pressure and velocity distributions in high- and superhigh-frequency acoustic waves. The range of measured pressures (in the given experiments 10–100 kPa) can be considerably widened by varying the defocusing length L. The spatial resolution of measurements is determined by the sizes of the CCD camera pixel, and at a minimum averaging window of 5×5 pixels and optical magnification $M = 1$ is about 40 μm. This value can also be decreased by varying the optical magnification. Reconstruction of the three-dimensional flow pattern in non-one-dimensional acoustic waves requires multiaspect probing and calculation of the local values with the use of integral transforms.

The authors wish to thank Prof. B. S. Rinkevichius for helpful discussions and recommendations and Candidates of Sciences N. B. Bazylev and E. I. Lavinskaya for assistance in developing programs for mathematical treatment of images.

This work was supported by INTAS (grant No. 05-1000007-425), the Belarusian Republic Basic Research Foundation (grants T07-070 and T07F-005), and the Royal Society of Edinburgh.

NOTATION

a, b, semiaxes of the diffraction halo ellipse, mm; c and c_∞, velocity of sound in an acoustic wave and a medium at rest; d_∞, speckle size at a "short" exposure, μm; D_x, D_y, projections of the axes of the diffraction halo ellipse on the coordinate axis, mm; D_∞, diffraction halo diameter in an unperturbed region, mm; $I(m, n)$, laser radiation intensity distribution in the speckle field, W/m^2; J_m, Bessel function of order m; k, acoustic wave vector magnitude; L, defocusing parameter, mm; l_z, optical path along the z-axis; (m, n), current coordinates in the initial image; M, optical magnification in speckle field imaging; n, optical refractive index of the medium; n_a, acoustic refractive index of the medium; p, pressure, Pa; r, radial coordinate; s, coordinate along the optical path; t, time, sec; T, temperature; (u, v), current coordinates in the Fourier plane; v, velocity, m/sec; x, y, z, spatial coordinates; β, piezooptical coefficient; ζ, Raman–Nath parameter; Δ, speckle displacement vector, μm; Δd_x, Δd_y, elongation of speckles in corresponding directions, μm; Δp_0, amplitude of pressure changes in the acoustic wave, Pa; Δn_0, amplitude of changes in the refractive index in the acoustic wave; ε_γ, deflection angle of the probing radiation along the y-axis due to refraction, rad; $\Delta\varepsilon_y$, amplitude of the probing radiation deflection angle along the y-axis due to refraction, rad; φ, phase of the acoustic wave; λ, laser radiation wavelength, μm; Λ_a, acoustic wavelength, mm; θ_m, laser radiation deflection angle for the diffraction order m, rad; θ_0, angle of incidence of the probing radiation, rad; $\tilde{\sigma}(m, n)$, experimental noise in the initial

intensity of the speckle field, W/m^2; $\sigma(u, v)$, experimental noise in the Fourier plane; σ_1, rms deviation of the laser radiation intensity, W/m^2; ω, acoustic wave frequency, sec^{-1}; $\mathbb{C}(m, n)$, contrast of the speckle field; $\mathbb{F}\{...\}$, Fourier transform operator; $\mathcal{I}(m, n)$, autocorrelation function of the speckle field. Subscripts: a, acoustic; ∞, parameters in the unperturbed region; m, diffraction order.

REFERENCES

1. A. Toepler, Optischen Studien nach der Methode der Schlierenbeobachtung, *Poggendorfs Ann. der Physik Chemie*, **131**, 33–35 (1867).
2. E. Mach und P. Salcher, Photographische Fixierung der Strömungsführung durch Projectile in der Luft eingeleiteten Vorgange, *Sitzungsb. Acad. Wiss. Wien*, **95**, 764–780 (1887).
3. W. H. F. Talbot, On the production of instantaneous images, *Philos. Mag.*, **34**, No. 1, 73–77 (1852).
4. G. S. Settles, *Schlieren and Shadowgraph Techniques. Visualizing Phenomena in Transparent Media*, Springer Verlag, New York (2001).
5. Yu. E. Nesterikhin and R. I. Soloukhin, *Methods of Rapid Measurements in the Gas Dynamics and Physics of Plasma* [in Russian], Nauka, Moscow (1967).
6. W. Merzkirch, *Flow Visualization*, 2nd ed., Academic Press, Orlando (1987).
7. V. F. Klimkin, A. N. Papyrin, and R. I. Soloukhin, *Optical Methods of Recording Fast Processes* [in Russian], Nauka, Novosibirsk (1980).
8. K. Takayama, Application of holographic interferometry to shock wave research, *Proc. SPIE*,**398**, 174–180 (1983).
9. G. Ben-Dor, O. Igra, and T. Elperin (Eds.), *Handbook of Shock Waves*, Academic Press, New York (2001).
10. N. Fomin, *Speckle Photography for Fluid Mechanics Measurements*, Springer Verlag, Berlin (1998).
11. N. A. Fomin, Diagnostics of fast processes in fluid, gas, and plasma mechanics, *Inzh.-Fiz. Zh.*, **81**, No. 1, 68–80 (2008).
12. T. S. Durrani and C. A. Greated (A. I. Bozhkov Ed.), *Laser Systems in Flow Measurements* [Russian translation], Énergiya, Moscow (1980).
13. B. S. Rinkevichius, *Laser Diagnostics of Flows* [in Russian], MÉI, Moscow (1990).
14. R. J. Adrian, Particle imaging technique for experimental fluid mechanics, *Annu. Rev. Fluid Mech.*, **23**, 261–304 (1991).
15. M. Raffel, C. Willert, and J. Kompenhans, *Particle Image Velocimetry: A Practical Guide*, Springer Verlag, Berlin (1998).
16. T. S. Durrani and C. A. Greated, Spectral analysis and cross-correlation techniques for the photon correlation technique, *Appl. Opt.*, **14**, No. 3, 778–786 (1975).
17. J. P. Sharpe and C. A. Greated, The measurement of periodic acoustic fields using photon correlation spectroscopy, *J. Phys. D: Appl. Phys.*, **20**, No. 2, 418–423 (1987).
18. D. B. Hann and C. A. Greated, The measurement of flow velocity and acoustic particle velocity using particle-image velocimetry, *Meas. Sci. Technol.*, **8**, No. 8. 1517–1522 (1997).
19. M. Campbell, J. A. Cosgrove, C. A. Greated, S. Jack, and D. Rockliff, Review of LDA and PIV applied to the measurement of sound and acoustic streaming, *Opt. Laser Technol.*, **32**, No. 3, 629–639 (2000).
20. N. A. Fomin, O. G. Penyazkov, P. P. Khramtsov, and E. I. Lavinskaya, 3D turbulence diagnostics by digital speckle photography and Talbot interferometry, in: *Proc. Int. Conf. on the Methods of Aerophysical Research ICMAR-2007*, Pt. IV, Novosibirsk (2007), pp. 22–27.
21. N. Fomin, E. Lavinskaya, M. Campbell, J. Cosgrove, C. Greated, and D. Skulina, Acoustical field diagnostics by digital laser speckle photography, in: *Proc. 25th Int. Symp. on Shock Waves — ISSW25*, Bangalor (2005), pp. 855–860.
22. C. Greated, J. Cosgrove, N. Fomin, and E. Lavinskaya, Sound measurement using speckle interferometry, *CD Proc. Forum Acusticum Conf.*, Budapest (2005).
23. N. Fomin, E. Lavinskaya, C. Greated, and J. Cosgrove, Quantitative visualization of acoustic waves by digital dynamic laser speckle photography, *CD Proc. 12th Int. Symp. on Flow Visualization*, Gottingen (2006).

24. E. I. Lavinskaya, S. A. Martem'yanov, J.-B. Solnier, and N. A. Fomin, Limited-projection laser tomography of complex gas dynamic flows, *Inzh.-Fiz. Zh.*, **77**, No. 5, 94–104 (2004).
25. N. Fomin, E. Lavinskaya, and K. Takayama, Limited-projection laser speckle tomography of complex flows, *Optics Lasers Eng.,* **44**, Nos. 3–4, 335–349 (2006).
26. A. R. Harland, *The Application of Laser Doppler Velocimetry to the Measurement of Underwater Acoustic Pressure Fields*, PhD Thesis, Badminton Press, Leicester, UK (2002).
27. H. Eisenberg, Equation for the refractive index of water, *J. Chem. Phys.*, **43**, No. 12, 3887–3892 (1965).
28. C. V. Raman and N. S. N. Nath, The diffraction of light by high frequency sound waves, *Proc. Indian. Acad. Sci.*, **3**, 75–84 (1936).
29. N. S. N. Nath, The diffraction of light by supersonic waves, *Proc. Indian. Acad. Sci.*, **8**, 499–503 (1938).
30. H. M. Colbert and K. L. Zankel, Light diffraction by ultrasonic wave — Fresnel region, *J. Opt. Soc. Am.*, **35**, No. 2, 359–363 (1963).
31. F. Kuliasko, R. Mertens, and O. Leroy, Diffraction of light by supersonic waves: the solution of the Raman-Nath equations, *Proc. Indian. Acad. Sci.*, **67A**, 295–302 (1968).
32. W. A. Riley, L. A. Love, and D. W. Griffith, Observation of Raman-Nath optical diffraction in the phase grating plane, *J. Opt. Soc. Am.*, **71**, No. 5, 1149 (1982).
33. E. Blomme and O. Leroy, Diffraction of light by ultrasound: finite analytical expressions for the spectra up to order 3, *Acustica*, **57**, 168–174 (1985).
34. P. Kwiek, W. Molkenstruck, and R. Reibold, Determination of the Klein-Cook parameter in ultrasound light diffraction, *Ultrasonics*, **34**, 801–805 (1996).
35. R. Reibold and W. Molkenstruck, Light diffraction tomography applied to the investigation of ultrasonic fields. Pt. 1. Continuous waves, *Acustica*, **56**, 180–192 (1984).
36. R. Reibold, Light diffraction tomography applied to the investigation of ultrasonic fields. Pt. 2. Standing waves, *Acustica*, **63**, 283–289 (1987).
37. R. Reibold and P. Kwiek, Extension of light-diffraction tomography beyond the weak acousto-optic interaction, *Acustica*, **81**, 43–52 (1995).
38. B. S. Rinkevichius, O. A. Evtikhieva, and I. L. Raskovskaya, Propagation of a Gaussian laser beam with elliptical cross-section through a medium in the presence of a standing acoustic wave, in: N. Fomin, O. Penyazkov, and S. Zhdanok (Eds.), *Physics of Shock Waves*, *Combustion*, *Detonation and Non-Equilibrium Processes*, Minsk (2005), ISBN-985-6456-47-9, pp. 64–65.
39. C. Greated, E. Lavinskaya, and N. Fomin, Numerical simulation of acoustical wave tracing, *Mat. Modelir.*, **15**, No. 7, 75–80 (2003).
40. N. B. Bazylev, E. I. Lavinskaya, S. P. Rubnikovich, and N. A. Fomin, *Digital Laser Speckle Anenometry in Microchannels* [in Russian], Preprint No. 8 of the Heat and Mass Transfer Institute, National Academy of Sciences of Belarus, Minsk (2006).
41. R. S. Sirohi, Speckle methods in experimental mechanics, in: R. S. Sirohi (Ed.), *Speckle Metrology*, Academic Press, New York (1993), pp. 99–155.
42. J. D. Briers, Speckle fluctuations as a screening test in the holographic measurements of plant motion, *J. Exp. Bot.*, **29**, 395–399 (1978).
43. A. F. Fercher and J. D. Briers, Flow visualization by means of single-exposure speckle photography, *Opt. Commun.*, **37**, 326–329 (1981).
44. J. D. Briers and S. Webster, Laser speckle contrast analysis (LASCA): a non-scanning, full-field technique for monitoring capillary blood flow, *J. Mod. Opt.*, **1**, 174–179 (1996).
45. N. B. Bazylev, N. A. Fomin, E. I. Lavinskaya, and S. P. Rubnikovich, Real-time blood micro-circulation analysis in living tissues by dynamic speckle technique, *Acta Bioeng. Biomech.*, **4**, suppl. 1, 510–511 (2002).
46. N. B. Bazylev, E. I. Lavinskaya, S. A. Naumovich, S. P. Rubnikovich, and N. A. Fomin, Quasi-real time, laser sounding of biotissues by the methods of dynamic speckle photography, *Dokl. Nats. Akad. Nauk Belarusi*, **47**, No. 4, 46–51 (2003).